HHS Public Access

Author manuscript

J Cardiovasc Comput Tomogr. Author manuscript; available in PMC 2018 June 05.

Published in final edited form as:

J Cardiovasc Comput Tomogr. 2011 ; 5(6): 459–466. doi:10.1016/j.jcct.2011.10.011.

A comparison of reconstruction and viewing parameters on image quality and accuracy of stress myocardial CT perfusion

Brian B. Ghoshhajra, MD, MBA[a,*], **Ian S. Rogers, MD, MPH**[a,b], **Pal Maurovich-Horvat, MD**[a], **Tust Techasith, MD**[a], **Daniel Verdini, MD**[a], **Manavjot S. Sidhu, MD**[a], **Nicola K. Drzezga, RT**[a], **Hector M. Medina, MD**[a], **Ron Blankstein, MD**[c], **Thomas J. Brady, MD**[a], and **Ricardo C. Cury, MD**[a,d]

[a]Cardiac MR PET CT Program, Department of Radiology and Division of Cardiology, Massachusetts General Hospital and Harvard Medical School, 165 Cambridge Street, Suite 400, Boston, MA, 02114, USA

[b]Division of Cardiovascular Medicine, Stanford University, Falk Cardiovascular Research Center, Stanford, CA, USA

[c]Non-Invasive Cardiovascular Imaging Program, Cardiovascular Division and Department of Radiology, Brigham and Women's Hospital, Boston, MA, USA

[d]Cardiovascular MRI and CT Program, Baptist Cardiac and Vascular Institute, Miami, FL, USA

Abstract

BACKGROUND—Myocardial stress computed tomography perfusion (CTP) has similar diagnostic accuracy for detecting perfusion defects (PDs) versus single-photon emission computed tomography (SPECT). However, the optimal diagnostic viewing and image processing parameters for CTP are unknown.

OBJECTIVE—We sought to compare the diagnostic accuracy of different image processing techniques, cardiac phases, slice thicknesses, and viewing parameters for detection of PDs.

METHODS—A stress and rest dual-source CTP protocol was performed with adenosine. Twelve subjects with severe stenosis proven by quantitative coronary angiography (QCA), with corresponding territorial defects at SPECT, were selected as well as 7 controls (subjects with similar clinical suspicion but negative QCA and SPECT). Short-axis stress images were processed with 3 techniques: minimum intensity projection (MinIP), maximum intensity projection, and average intensity multiplanar reconstruction (MPR), 3 thicknesses (1, 3, 8 mm), and 2 phases (systolic, mid-diastolic). The resulting images (n = 1026) were randomized and interpreted by independent readers.

RESULTS—Diastolic reconstructions (8-mm MPR) showed the highest sensitivity (81%) to detect true PDs. The highest accuracy was achieved with the 8-mm (61%) and 1-mm (61%) MPR diastolic images. The most sensitive and accurate systolic reconstructions were 3-mm MinIP

*Corresponding author. bghoshhajra@partners.org.

Conflict of interest: Astellas Pharmaceuticals Inc. provided grant support for the initial study. The authors maintained full control over this study design and data.

images. These findings related to viewing in relatively narrow window width and window level settings.

CONCLUSION—Viewing parameters for optimal accuracy in detection of perfusion defects on CTP differ for systolic and diastolic images.

Keywords

Optimal viewing parameters; Cardiac computed tomography; Perfusion defects

Introduction

Myocardial stress computed tomography perfusion (CTP) is capable of identifying fixed and reversible myocardial perfusion defects (PDs) by imaging during contrast injection under pharmacologic stress. Single-center CTP feasibility trials have shown similar accuracy to single-photon emission CT (SPECT) myocardial perfusion imaging (MPI) and invasive coronary angiography (ICA).[1,2] Moreover, CTP can be used to significantly improve the diagnostic accuracy of CT angiography (CTA) to detect hemodynamically significant stenosis among patients with an intermediate-to-high risk of obstructive coronary artery disease (CAD).[3]

The optimal parameters for interpreting CTP examinations have not yet been carefully evaluated. Although CTP dataset acquisition is similar to techniques used for standard electrocardiographically gated CTA, there has been no controlled evaluation of the myocardium with the use of various image processing and viewing parameters.

A wide array of reconstruction and viewing tools exist for the review of coronary CTA examinations. The 3 dimensional datasets can be displayed in any desirable plane or slice thickness, ranging from simple review of contiguous axial images to settings that range from multiplanar reformatted (MPR) images to curved multiplanar techniques, maximum intensity projections (MIP), minimum intensity projections (MinIP), and volume-rendering techniques. Prior published data and experience with conventional cardiac CTA favor a combination of axial image review, augmented by multiplanar techniques with occasional use of MIP images.[4] The goal of each of these techniques is to display the vessel in question with adequate signal to noise, without introducing artifacts or misrepresenting the degree of luminal narrowing.

In contrast, CTP aims solely to evaluate true differences in myocardial iodine density during a first-pass contrast administration at stress and rest. Preliminary experience suggests the use of thicker slices, average MPR or MinIP reconstructions, the use of narrow window width (WW) and window level (WL) for image display, and the evaluation of multiple cardiac phases.[5,6] However, the optimal image processing display parameters for interpreting CTP examinations have not been systematically evaluated. Furthermore, the optimal phase in the cardiac cycle (ie, systole or diastole) for accurately identifying PDs is currently unknown. Therefore, the aim of this study was to evaluate various image processing parameters to determine the optimal display settings for visualizing CTP defects. Specifically, we sought

to compare the diagnostic accuracy of different image processing techniques, cardiac phases, and slice thicknesses for the detection of true PDs.

Methods

Images were obtained as part of a feasibility trial in which patients underwent stress and rest myocardial CTP with first-generation dual-source cardiac CT. Recruited patients had an intermediate-to-high likelihood of CAD and previously underwent SPECT and ICA. Our institutional review board approved the study protocol. Written informed consent was obtained before subject enrollment. HIPAA compliance was maintained. The data were also reported previously in separate analyses of a larger series of patients used to validate the modality's feasibility and accuracy compared with quantitative coronary angiography (QCA) and SPECT MPI,[1] the incremental value of CTP to CTA,[3] and the interscan reliability compared with SPECT MPI.[7] Astellas Pharma (Deerfield, IL) provided partial support, supplying the adenosine and research grant support. The authors had full control of the data obtained and the statistical analysis.

Study subjects

In this study, a cohort of patients was prospectively enrolled for assessment of the feasibility of CTP under pharmacologic stress. Patients >40 years of age who underwent SPECT, with a high clinical likelihood of subsequent ICA, and patients who underwent SPECT and ICA without intervention were recruited. Exclusion criteria were acute clinical instability, contraindication to adenosine (eg, advanced heart block, asthma, critical aortic stenosis, systolic blood pressure < 90 mm Hg) or iodinated contrast (known allergy, serum creatinine > 1.5 mg/dL), pregnancy, and atrial fibrillation. Twelve subjects with clear severe stenosis (≥ 70% by QCA) with a corresponding territorial SPECT defect were selected, as well as 7 controls with no evidence of significant CAD (no epicardial coronary narrowing > 40% luminal narrowing and no history of myocardial infarction).

Stress myocardial CTP protocol

CTP was performed with a dual-source scanner (Somatom Definition; Siemens Medical Solutions, Forchheim, Germany). Intravenous catheters were placed in both antecubital veins: a right 20-gauge catheter for adenosine (Astellas Pharma) infusion and a left 18-gauge catheter for contrast injection. After scout images, contrast timing was determined by test bolus injection: 10 mL of contrast (370 mg of iopamidol/mL, Isovue 370; Bracco Diagnostics, Princeton, NJ) at 4 mL/sec, followed by 20-mL saline flush. Adenosine infusion was then administered at 140 7μg/kg/min for ≥3 minutes. Stress scanning was performed from the carina to the diaphragm with helical-mode retrospective electrocardiographic (ECG) gating.

Stress CTP was acquired at 2 × 32 × 0.6 mm (number of x-ray sources × number of detector slices × slice thickness) with the use of a gantry rotation time of 330 milliseconds with a half-scan reconstruction algorithm (temporal resolution, 83 milliseconds). A z-flying focal spot was used to obtain 64 slices in retrospective-gated modes. Images were acquired without use of β-blockers or nitroglycerine vasodilation to maximize the effects of the

pharmacologic stress agent.[8] The tube voltage was selected according to the body mass index (BMI): 100 kV for BMI < 30 kg/m^2 and 120 kV for BMI ≥ 30 kg/m^2. Tube current was varied from 330 to 370 mA according to patient size. ECG-based tube current modulation was implemented with a pulsing window of 60%–70% of the R-R interval for peak reference milliampere, and 20% of the peak reference milliampere for the remainder of the R-R cycle. Automatic heart rate–based adaptive pitch selection (0.2–0.5) was enabled. Iopamidol was injected at 4–5 mL/sec according to the scanning duration (approximately 65 mL). Throughout adenosine infusion, symptoms, heart rate, blood pressure, ECG readings, and rhythm strips were registered and monitored by an Advanced Cardiac Life Support–certified radiologist or cardiologist.

Immediately after stress acquisition, adenosine infusion was discontinued. Five minutes were allotted to allow the heart rate to return to baseline and to ensure resolution of any symptoms before rest CTP imaging. Axial-mode prospectively ECG-triggered (Siemens Sequential Scanning) acquisition centered at 65% of the R-R interval was then performed with a tube current that varied from 150 to 258 mA and a section thickness of 0.75 mm (collimation, 32 × 0.75 mm). The same tube voltage (100 or 120 kV) and approximately the same contrast material volume (65–70 mL) were used for stress and rest image acquisitions. In some cases, rest acquisition required ≤ 70 mL of contrast to allow for a longer scan time because of table movement and ECG synchronization on every second heartbeat. Radiation dose includes the stress and rest phase imaging; retrospectively gated stress examinations were performed with automated milliampere selection when body habitus allowed. Total effective dose was calculated as the product of the dose length product and a conversion coefficient for the chest (κ = 0.014 mSv/mGy · cm).[9]

Fifty subjects underwent a feasibility trial of CTP,[1] of which 43 underwent both SPECT and ICA in addition to CTP. For this substudy, cases with concordant territorial SPECT and angiographic defects, or lack thereof (as determined by research interpretations and QCA) were selected. Twelve subjects with severe stenosis (≥ 70% by QCA) with a corresponding territorial SPECT defect were selected, as well as 7 controls with no evidence of significant CAD (no epicardial coronary narrowing >40% or no history of infarct by QCA and SPECT) (Fig. 1).

Short-axis left ventricular stress CTP images were reconstructed with a B25 smooth kernel with 3 image processing techniques (MinIP, MPR, and MIP) and 3 slice thicknesses (1, 3, and 8 mm), and at 2 phases of the cardiac cycle (35% and 65% R-R interval, representing systole and diastole, respectively). Images were then selected specifically at the mid, apical, and basal levels, separately yielding 3 short-axis slices for each case. Images were not grouped on a per-patient basis but rather were separately saved as individual DICOM images with the above-mentioned parameters. An example of the various reconstructions through a defect is shown in Figure 2. The 1026 resulting individually reconstructed slices were then randomized, and all identifying data, including descriptors of slice thickness and image type, were removed from the image headers.

Average MPR and MinIP reconstructions were chosen on the basis of prior published experiences.[1] MIP reconstructions are another commonly used reconstruction in cardiac

imaging, and we included these images as well, although we hypothesized that this image type could potentially mask a defect by projecting adjacent high-density voxels over low-density voxels within the same slab.

Data analysis

Two experienced investigators (B.B.G. and P.M.H., level 3 trained in cardiac CT) independently analyzed the randomized, blinded CTP datasets. Reader 1 interpreted the entire dataset; reader 2 interpreted a subset for interreader agreement purposes. The readers were blinded to the case selection and image set creation. Images were interpreted on an independent workstation (Osirix 3.6.1, Geneva, Switzerland) in ambient light conditions similar to that of clinical reading conditions. Readers were provided only the short-axis images and allowed to adjust the WW and WL to their own preference. The standard American College of Cardiology-American Heart Association 17-segment model for standardized myocardial segmentation was used for image interpretation.[10]

Image sets were interpreted for the presence or absence of defects, and the location of these defects (see Fig. 2). For each defect, the severity and reversibility were recorded on a 4-point scale (severity: none, mild, moderate, severe; reversibility: none, minimal, partial, complete). Image quality and reader confidence were each graded on a 4-point scale (image quality: 1 poor/uninterpretable, 2 moderate, 3 good, 4 excellent; confidence: 1 no confidence, 2 low, 3 moderate, 4 very confident). Readers also recorded the final WW and WL used for image display when interpreting each image.

SPECT MPI protocol

The SPECT images were acquired according to the standard institutional protocol.

Reference standard

QCA was considered the reference standard and was performed offsite, at an independent core laboratory (Harrington McLaughlin Heart and Vascular Institute, Case Western Reserve University, Cleveland, Ohio). The percentage diameter of stenosis was calculated with an automated contour detection algorithm (CAAS II Analysis System; Pie Medical, Maastricht, the Netherlands) in ≥ 2 orthogonal angiographic views. Cases were included in the analysis when there was ≥ 70% luminal narrowing in one of the epicardial coronary arteries, with a corresponding defect on nuclear SPECT imaging.

Statistical analyses

Continuous variable data are reported as means ± SD or medians as appropriate. Categorical variable data are presented as percentages. The diagnostic accuracy of each CTP dataset reconstruction for the detection of severe stenosis, with matched QCA/SPECT result as the reference standard, was expressed as sensitivity, specificity, positive predictive value, negative predictive value, and accuracy. Calculations were performed on both a per-vessel (left anterior descending, left circumflex, and right coronary arteries) basis and a per-patient basis. A P value < 0.05 at 2-tailed probability analysis was considered to indicate statistical significance. All statistical analyses were performed with SAS 9.2 (SAS Institute Inc, Cary, NC).

Results

Patient characteristics

Patient characteristics are summarized in Table 1. No differences were observed between cases or controls for demographic or clinical variables, except for history of myocardial infarction as per study design.

Diagnostic accuracy

Per-patient diagnostic accuracy is shown in Table 2. A most sensitive reconstruction method in diastole was average MPR at 8-mm thickness with sensitivity of 81%. In diastole, a highest accuracy (61%) was achieved in average MPR 8 mm and 1 mm.

In systole a highest specificity of 95% was seen in 3-mm MinIP. A highest sensitivity of 42% was also seen in 3-mm MinIP. In systole a highest accuracy in systole (61%) was seen in MinIP 3-mm images.

Interreader agreement for the presence of any PD was calculated on a per-patient basis, showing moderate agreement (Cohen's κ of 0.54). On a per-vessel territory basis, MPR 8-mm diastolic images yielded a sensitivity of 56%, whereas MinIP 3-mm images yielded a specificity of 98%, as well as the accuracy of 81% (Table 2).

Image quality and reader confidence

The readers' subjective rating of both image quality and diagnostic confidence was not significantly different for the cases whose blinded interpretation was read "correctly" (agreement with the combined reference standard) compared with cases whose blinded interpretation was incorrect (disagreement). Median image quality score for correct cases (n = 567) and incorrect cases (n = 459) was 2. The confidence level score for both correct and incorrect cases was 2.

The preferred WW and WL are listed per reconstruction method in Table 3. Reader preference favored display settings characterized as a narrow WW and WL, with levels that varied slightly for each case but maintained average ratios of between 1.5 and 3.0.

Discussion

In this analysis of imaging parameters in a cohort of patients with hemodynamically significant coronary stenosis confirmed by QCA and SPECT, we determined the optimal diagnostic viewing parameters with each phase of cardiac cycle used for the detection of CTP defects. In diastole, CTP defects were most optimally visualized with 8-mm short-axis slices displayed with average intensity multiplanar reformation. We found that image quality and confidence directly correlate with reader accuracy. Optimal display setting for visualization of myocardial PDs include a narrow WW and WL, with a ratio (WW/WL) of approximately 2:1 being preferable.

Previous works have established that CTP is feasible, safe, and has comparable diagnostic accuracy and radiation dose to SPECT and augments the diagnostic accuracy of CTA in

high-risk patients.[1,3,7] Other work has evaluated the subjective and quantitative use of resting CT for infarct detection.[11] This study adds significant information to the existing literature on CTP by providing data on the optimal viewing parameters for CTP datasets, which are inherently different because of key differences in acquisition methods.

Appropriate use of these parameters is important for clinical evaluation of myocardial perfusion and may also serve as a guide for future research in this newly emerging field. Such knowledge may be particularly important because advances in cardiac CT are expected to pave the road for the clinical utilization of CTP. For instance, acquisition speeds of advanced scanners now allow subsecond imaging of the thorax with or without ECG gating, and myocardial analysis may soon become part of a comprehensive evaluation of patients presenting with chest pain.[12,13]

Our study showed highest accuracy with the use of 1-mm and 8-mm MPR reconstructions in diastole, as well as 3-mm MinIP in systole. In a clinical situation, several image types may prove helpful. For example, MinIP images lend specificity at the expense of sensitivity and therefore might serve as a good tool for confirmation after initial detection with MPR images, the reconstructions which showed highest sensitivity. The ideal viewing parameters may actually be a combination of several reconstructions, just as various complementary image sequences are used in a single MRI interpretation.

However, certain limitations to our research must be noted. The comparisons we made apply only to single short-axis slices, a comparison designed to isolate the effects of slice reconstruction alone. In the clinical reading room, interpreting physicians have the luxury of volume datasets and numerous contiguous slices. This study describes the relative accuracies of different techniques used in the clinical interpretation of CTP. The absolute accuracy of these techniques within clinical practice is the subject of ongoing study. We used a first-generation dual-source CT scanner, with high temporal resolution, but narrow z-axis coverage (maximum 19.2 mm in helical thin slice mode or 28.8 mm in axial thick slice mode). Thicker reconstructions can mitigate subtle slab artifacts and motion artifacts, which are inherent to this relatively short z-axis coverage. Newer scanners offer improved temporal resolution and wider detector arrays, which may obviate the benefits of thicker slice reconstructions. However, our findings may still prove useful to help exploit the relatively small difference in iodine concentrations at first-pass imaging.[14]

Image noise remains a problem with ECG-gated CT, in part because of the half-scan interpolation algorithm necessary to maintain satisfactory temporal resolution. Ideal reconstruction parameters mitigate the effects of noise and improve the contrast-to-noise ratio. In the future, novel reconstruction methods such as iterative reconstruction may fundamentally change the way images are created, thereby suppressing noise.[15]

Our protocol tightly controlled radiation doses. We implemented ECG-based milliampere modulation, and, when possible, we used tube potentials of 100 kV and scout image-based milliampere modulation for retrospective acquisitions. Therefore, all systolic reconstructions were inherently photon starved because they were intentionally obtained at only 20% of the peak diastolic reference milliampere. The sensitivity of our systolic-phase images may be

confounded by low-dose technique and image noise. Despite this, our results were relatively favorable in systole; because of the inherent differences in diastolic and systolic acquisitions as a result of pulsing, our data do not allow for direct comparison of sensitivities between diastolic and systolic stress imaging.

We chose to evaluate 65% R-R interval reconstructions for diastolic images, because mid-late diastolic images are commonly used for CTA acquisition and interpretation; these may not always be the most ideal motion-free phase to evaluate the myocardium, particularly at higher heart rates. We chose this phase to allow direct comparison of stress and rest images (which were prospectively triggered at 65% R-R interval) for our larger study.

Our analysis did not include a side-by-side comparison of images (which might better elucidate subjective reader preferences). We chose not to explore the potential effects of different color and gray-scale mappings of the CT images. Finally, the use of ≥ 70% stenosis by QCA (with corresponding SPECT defects) in these cases was not confirmed with functional flow reserve at ICA. This retrospective study inherits the limitations of selection bias and a small sample size, factors we tried to mitigate by the independent, blinded, random interpretation of each slice. We made only subjective assessments involving 2 reviewers, although a separately performed, objective quantitative approach could potentially complement this work. The effects of image noise might then be separated from the effects of slice thickness. The actual sensitivity, specificity, and accuracy of these isolated, single-slice interpretations cannot be generalized to actual volume dataset interpretations as would be performed in clinical patients.

Conclusion

In summary, in this analysis of a selected dataset of CTP cases with concordant QCA and SPECT findings (i.e., defects because of severe stenoses and normals without significant stenoses), our findings suggest that the optimal parameters for myocardial analysis included diastolic phase images reconstructed at thicker slices on average intensity MPR projections, or systolic phase, thinner MinIP projections. Although readers and patients each may prefer a unique display WW and WL, a narrow WW and WL (a helpful starting point is approximately WW 200 HU), with approximate ratio of WW/WL of 2:1 may be most useful for CTP interpretation.

Acknowledgments

We thank the referring cardiologists of The Massachusetts General Hospital, the Nuclear Medicine Department, and the CT Department and Technologists.

Contributing investigators

We acknowledge the many collaborators who assisted in the collection of this data, including Leon Shturman, DO, Jose Rocha-Filho, MD, David Okada, BA, Ammar Sarwar, MD, Anand V. Soni, MD, Hiram Bezerra, MD, Milena Petranovic, MD, Ricardo Loureiro, MD, Gudrun Feuchtner, MD, Henry Gewirtz, MD, Udo Hoffmann, MD, MPH, and Wilfred S. Mamuya, MD, PhD.

References

1. Blankstein R, Shturman LD, Rogers IS, Rocha-Filho JA, Okada DR, Sarwar A, Soni AV, Bezerra H, Ghoshhajra BB, Petranovic M, Loureiro R, Feuchtner G, Gewirtz H, Hoffmann U, Mamuya WS, Brady TJ, Cury RC. Adenosine-induced stress myocardial perfusion imaging using dual-source cardiac computed tomography. J Am Coll Cardiol. 2009; 54:1072–1084. [PubMed: 19744616]
2. George RT, Arbab-Zadeh A, Miller JM, Kitagawa K, Chang H-J, Bluemke DA, Becker L, Yousuf O, Texter J, Lardo AC, Lima JA. Adenosine stress 64- and 256-row detector computed tomography angiography and perfusion imaging: a pilot study evaluating the transmural extent of perfusion abnormalities to predict atherosclerosis causing myocardial ischemia. Circ Cardiovasc Imaging. 2009; 2:174–182. [PubMed: 19808590]
3. Rocha-Filho JA, Blankstein R, Shturman LD, Bezerra HG, Okada DR, Rogers IS, Ghoshhajra B, Hoffmann U, Feuchtner G, Mamuya WS, Brady TJ, Cury RC. Incremental value of adenosine-induced stress myocardial perfusion imaging with dual-source CT at cardiac CT angiography. Radiology. 2010; 254:410–419. [PubMed: 20093513]
4. Ferencik M, Ropers D, Abbara S, Cury RC, Hoffmann U, Nieman K, Brady TJ, Moselewski F, Daniel WG, Achenbach S. Diagnostic accuracy of image postprocessing methods for the detection of coronary artery stenoses by using multidetector CT. Radiology. 2007; 243:696–702. [PubMed: 17517929]
5. Cury RC, Nieman K, Shapiro MD, Butler J, Nomura CH, Ferencik M, Hoffmann U, Abbara S, Jassal DS, Yasuda T, Gold HK, Jang I-K, Brady TJ. Comprehensive assessment of myocardial perfusion defects, regional wall motion, and left ventricular function by using 64-section multidetector CT. Radiology. 2008; 248:466–475. [PubMed: 18641250]
6. Blankstein R, Rogers IS, Cury RC. Practical tips and tricks in cardiovascular computed tomography: diagnosis of myocardial infarction. J Cardiovasc Comput Tomogr. 2009; 3:104–111. [PubMed: 19332342]
7. Okada DR, Ghoshhajra BB, Blankstein R, Rocha-Filho JA, Shturman LD, Rogers IS, Bezerra HG, Sarwar A, Gewirtz H, Hoffmann U, Mamuya WS, Brady TJ, Cury RC. Direct comparison of rest and adenosine stress myocardial perfusion CT with rest and stress SPECT. J Nucl Cardiol. 2010; 17:27–37. [PubMed: 19936863]
8. Taillefer R, Ahlberg AW, Masood Y, White CM, Lamargese I, Mather JF, McGill CC, Heller GV. Acute beta-blockade reduces the extent and severity of myocardial perfusion defects with dipyridamole Tc-99m sestamibi SPECT imaging. J Am Coll Cardiol. 2003; 42:1475–1483. [PubMed: 14563595]
9. Halliburton SS, Abbara S, Chen MY, Gentry R, Mahesh M, Raff GL, Shaw LJ, Hausleiter J. SCCT guidelines on radiation dose and dose-optimization strategies in cardiovascular CT. J Cardiovasc Comput Tomogr. 2011; 5:198–224. [PubMed: 21723512]
10. Cerqueira MD. Standardized myocardial segmentation and nomenclature for tomographic imaging of the heart: a statement for healthcare professionals from the Cardiac Imaging Committee of the Council on Clinical Cardiology of the American Heart Association. Circulation. 2002; 105:539–542. [PubMed: 11815441]
11. Rogers IS, Cury RC, Blankstein R, Shapiro MD, Nieman K, Hoffmann U, Brady TJ, Abbara S. Comparison of postprocessing techniques for the detection of perfusion defects by cardiac computed tomography in patients presenting with acute ST-segment elevation myocardial infarction. J Cardiovasc Comput Tomogr. 2010; 4:258–266. [PubMed: 20579617]
12. Boroto K, Remy-Jardin M, Flohr T, Faivre J-B, Pansini V, Tacelli N, Schmidt B, Gorgos A, Remy J. Thoracic applications of dual-source CT technology. Eur J Radiol. 2008; 68:375–384. [PubMed: 18929452]
13. Tacelli N, Remy-Jardin M, Flohr T, Faivre J, Delannoy V, Duhamel A, Remy J. Dual-source chest CT angiography with high temporal resolution and high pitch modes: evaluation of image quality in 140 patients. Eur Radiol. 2010; 20:1188–1196. [PubMed: 19890644]
14. Higgins CB, Sovak M, Schmidt W, Siemers PT. Uptake of contrast materials by experimental acute myocardial infarctions: a preliminary report. Invest Radiol. 1978; 13:337–339. [PubMed: 689828]
15. Sunnegårdh J, Danielsson P-E. Regularized iterative weighted filtered backprojection for helical cone-beam CT. Med Phys. 2008; 35:4173–4185. [PubMed: 18841870]

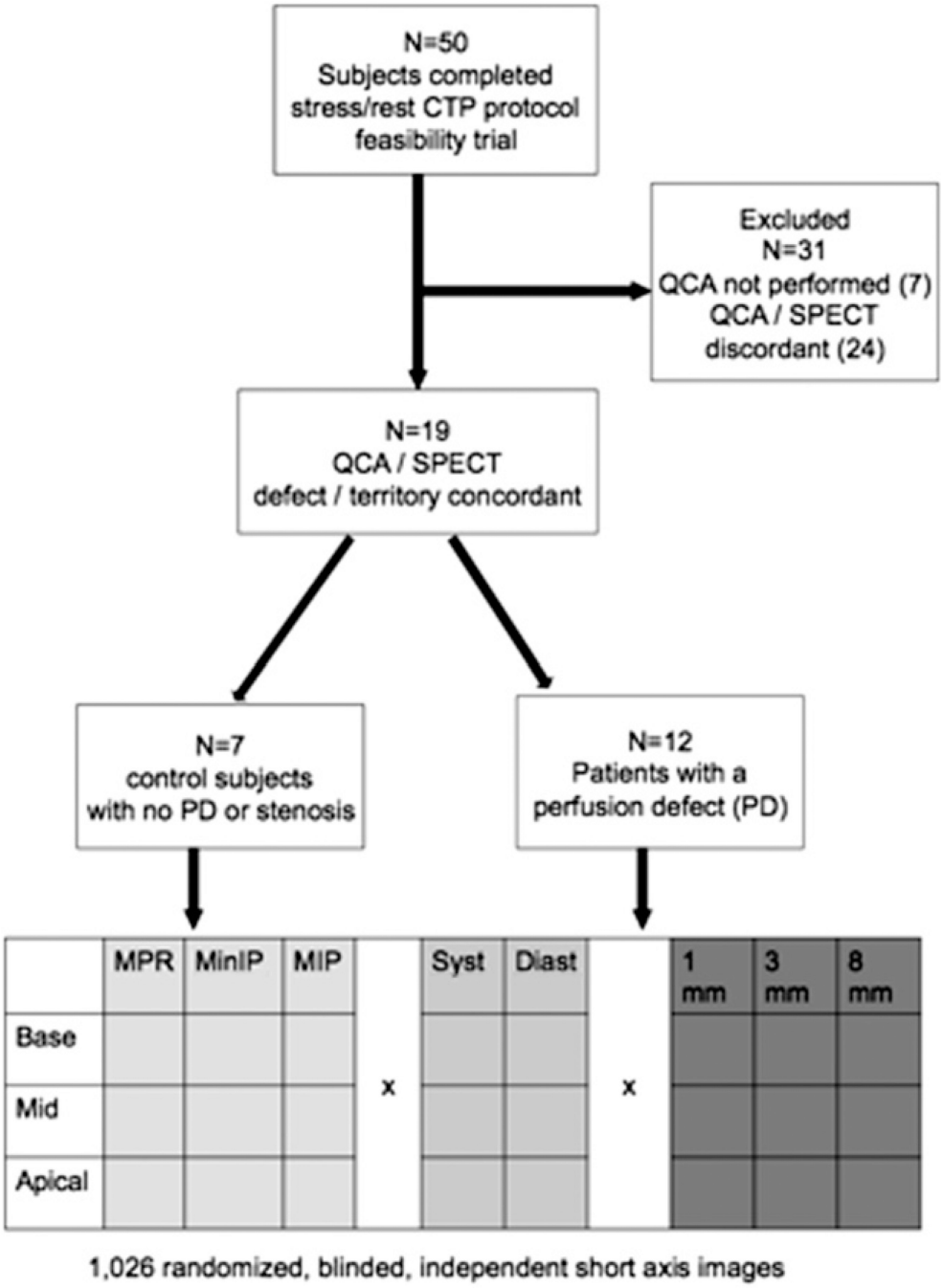

Figure 1.

Inclusion/exclusion criteria and image randomization process: 50 subjects underwent initial feasibility trial of CTP, of which subjects were excluded because of QCA not being performed (n = 7), or discordance between defect territory between QCA and SPECT (n = 24). Of the remaining 19 subjects, 7 served as controls (ie, no significant defects at SPECT or no evidence of stenosis > 50% by QCA), and 12 served as positive cases (≥ 50% QCA, with a matching, at least moderate perfusion defect in the same territory at SPECT).

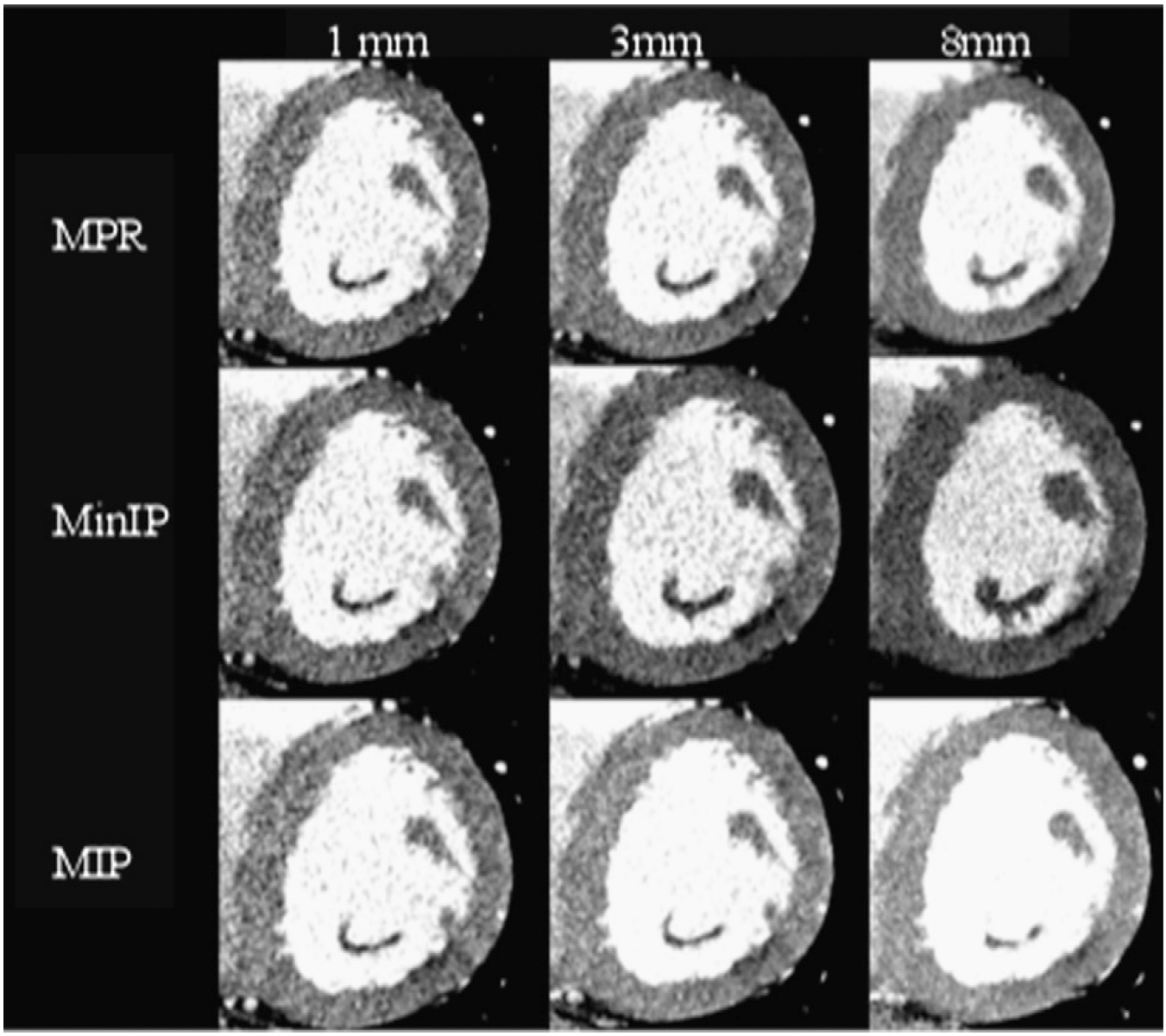

Figure 2.

Effect of multiple reconstruction parameters on image characteristics: MPR (top row), MinIP (middle row), and MIP (bottom row) short-axis reconstructions through the same apical segment defect in the inferolateral wall of the left ventricle. The patient had subtotal circumflex occlusion at invasive angiography, as well as a corresponding inferolateral wall reversible defect on SPECT imaging. In this figure, display WW and WL are held constant (200/100).

Table 1

Demographics

	Cases (n=12)	Controls (n=7)	*P*
Risk factor or demographic feature			
Age, y, mean ± SD	58.1 ± 10.6	59.8 ± 6.8	0.85
Male patients (%)	83	40	0.07
Diabetes mellitus (%)	25	0	0.28
Hypertension (%)	100	71	0.27
Dyslipidemia (%)	83	57	0.23
Obesity (%) *	50	29	0.39
Family history of CAD (%)	58	43	0.54
BMI, kg/m^2, mean ± SD	30.8 ± 4.2	28.0 ± 5.9	0.54
Smoking history (%)	58	43	0.34
Medical history			
Previous angina pectoris (%)	75	57	0.45
Prior myocardial infarction (%)	75	0	0.01
Prior coronary revascularization (%)	50	43	0.78
Lipid levels, mg/dL			
Total cholesterol, mean ± SD	171.7 ± 56.4	195.0 ± 47.0	0.08
HDL cholesterol, mean ±SD	45.6 ± 17.6	62.4 ± 28.6	0.07
LDL cholesterol, mean ±SD	101.5 ± 63.9	121.6 ± 33.4	0.10
Serum triglyceride, mean ± SD	143.3 ± 87.1	136.7 ± 73.0	0.87
Radiation dose			
Total mSv for rest and stress imaging, mean ± SD	11.8 ± 4.5	9.0 ± 2.5	0.26

CAD, coronary artery disease; BMI, body mass index; HDL, high-density lipoprotein; LDL, low-density lipoprotein.

Note: Family history, diabetes, and dyslipidemia were classified according to documentation in the cardiologist's notes.

* Obesity was defined as a BMI ≥ 30 kg/m^2.

Table 2

Diagnostic characteristics of different reconstruction methods per patient and per vessel

Reconstruction	Sensitivity, % (95% CI)	Specificity, % (95% CI)	ppv, % (95% CI)	NPV, % (95% CI)	Accuracy, % (95% CI)
Per patient					
Diastole (65%)					
MPR, 1 mm	61 (43–77)	62 (38–82)	73 (54–88)	48 (29–68)	61 (48–74)
MPR, 3 mm	67 (49–81)	33 (15–57)	63 (46–74)	37 (16–62)	54 (41–68)
MPR, 8 mm	81 (64–92)	29 (11–52)	66 (50–80)	46 (31–58)	61 (48–74)
MinIP, 1 mm	67 (49–81)	48 (26–70)	69 (51–83)	45 (24–68)	60 (46–72)
MinIP, 3 mm	58 (41–74)	62 (38–82)	72 (53–87)	46 (28–66)	60 (46–72)
MinIP, 8 mm	50 (33–67)	52 (30–74)	64 (44–81)	38 (21–58)	51 (37–64)
MIP, 1 mm	64 (46–74)	43 (22–66)	66 (48–81)	41 (21–64)	56 (42–69)
MIP, 3 mm	53 (46–79)	35 (15–57)	62 (45–78)	35 (15–59)	53 (39–66)
MIP, 8 mm	56 (38–72)	48 (26–70)	65 (45–81)	38 (20–59)	53 (39–66)
Systole (35%)					
MPR, 1 mm	33 (19–51)	90 (70–99)	86 (57–98)	44 (29–60)	54 (41–68)
MPR, 3 mm	39 (23–57)	81 (58–95)	78 (52–94)	44 (29–60)	54 (41–68)
MPR, 8 mm	39 (23–57)	71 (48–89)	70 (46–88)	41 (25–58)	51 (37–64)
MinIP, 1 mm	33 (19–51)	81 (58–95)	75 (48–93)	41 (26–58)	51 (37–74)
MinIP, 3 mm	42 (26–59)	95 (76–100)	94 (70–100)	49 (233.65)	61 (48–74)
MinIP, 8 mm	36 (21–54)	76 (53–92)	72 (47–90)	41 (26–58)	51 (37–64)
MIP, 1 mm	39 (23–57)	81 (58–95)	78 (52–94)	44 (28–60)	54 (41–68)
MIP, 3 mm	42 (26–59)	76 (53–92)	75 (51–91)	43 (27–61)	54 (41–68)
MIP, 8 mm	36 (21–54)	86 (64–97)	81 (54–96)	44 (28–60)	54 (41–68)
Per vessel					
Diastole (65%)					
MPR, 1 mm	47 (43–77)	78 (38–82)	47 (54–88)	78 (29–68)	68 (48–74)
MPR, 3 mm	51 (49–81)	58 (15–57)	34 (46–74)	74 (16–62)	56 (41–68)
MPR, 8 mm	56 (64–92)	55 (11–52)	35 (50–80)	74 (31–58)	55 (48–74)
MinIP, 1 mm	47 (49–81)	73 (26–70)	42 (51–83)	76 (24–68)	65 (46–72)
MinIP, 3 mm	41 (41–74)	74 (38–82)	40 (53–87)	75 (28–66)	64 (46–72)

Reconstruction	Sensitivity, % (95% CI)	Specificity, % (95% CI)	ppv, % (95% CI)	NPV, % (95% CI)	Accuracy, % (95% CI)
MinIP, 8 mm	35 (33–67)	76 (30–74)	37 (44–81)	74 (21–58)	64 (37–64)
MIP, 1 mm	49 (46–74)	73 (22–66)	43 (48–81)	77 (21–64)	65 (42–69)
MIP, 3 mm	47 (46–79)	64 (15–57)	36 (45–78)	74 (15–59)	59 (39–66)
MIP, 8 mm	44 (38–72)	72 (26–70)	39 (45–81)	76 (20–59)	64 (39–66)
Systole (35%)					
MPR, 1 mm	25 (14–40)	97 (92–99)	76 (50–93)	75 (68–82)	75 (68–82)
MPR, 3 mm	37 (24–52)	93 (86–97)	68 (48–84)	78 (70–84)	76 (69–82)
MPR, 8 mm	41 (28–56)	87 (79–92)	57 (39–73)	78 (70–84)	73 (66–80)
MinIP, 1 mm	27 (16–42)	93 (86–97)	61 (39–80)	75 (67–82)	73 (66–80)
MinIP, 3 mm	41 (28–56)	98 (93–99)	88 (68–97)	80 (72–86)	81 (74–86)
MinIP, 8 mm	29 (17–44)	89 (82–94)	54 (34–72)	75 (67–82)	71 (64–78)
MIP, 1 mm	33 (21–48)	95 (89–98)	74 (52–90)	77 (69–84)	77 (70–83)
MIP, 3 mm	43 (29–58)	91 (84–95)	67 (48–82)	79 (71–85)	77 (70–83)
MIP, 8 mm	29 (17–44)	93 (87–97)	65 (43–84)	76 (68–82)	74 (67–81)

PPV, positive predictive value; NPV, negative predictive value.

Table 3

Preferred window width (WW) and window level (WL) per image reconstruction type

Reconstruction	WW	WL	Ratio WW/WL
Average MPR, 1 mm	308 ± 86	165 ± 205	2.1 ± 0.5
MinIP, 1 mm	307 ± 77	141 ± 38	2.2 ± 0.5
MIP, 1 mm	305 ± 85	156 ± 41	2.0 ± 0.3
Average MPR, 3 mm	276 ± 84	144 ± 39	1.9 ± 0.4
MinIP, 3 mm	277 ± 70	129 ± 113	2.6 ± 1.0
MIP, 3 mm	303 ± 78	181 ± 53	1.7 ± 0.3
Average MPR, 8 mm	287 ± 90	105 ± 44	3.0 ± 1.1
MinIP, 8 mm	290 ± 77	188 ± 40	1.5 ± 0.3
MIP, 8 mm	290 ± 77	188 ± 40	1.5 ± 0.3

Note: Values are as mean ± SD.